Carbohydrate Polymers 90 (2012) 361–369

Contents lists available at SciVerse ScienceDirect

Carbohydrate Polymers

journal homepage: www.elsevier.com/locate/carbpol

Synthesis of β-cyclodextrin modified chitosan–poly(acrylic acid) nanoparticles and use as drug carriers

Xue Wang[a], Changjing Chen[b], Da Huo[a], Hanqing Qian[b], Yin Ding[c], Yong Hu[a,*], Xiqun Jiang[b,*]

[a] Nanjing National Laboratory of Microstructure, Department of Material Science & Engineering, Nanjing University, Nanjing 210093, PR China
[b] Laboratory of Mesoscopic Chemistry and Department of Polymer Science & Engineering, College of Chemistry & Chemical Engineering, Nanjing University, Nanjing 210093, PR China
[c] State Key Laboratory of Analytical Chemistry for Life Science, School of Chemistry and Chemical Engineering, Nanjing University, Nanjing 210093, PR China

ARTICLE INFO

Article history:
Received 18 November 2011
Received in revised form 10 May 2012
Accepted 18 May 2012
Available online 28 May 2012

Keywords:
Chitosan
Cyclodextrin
Nanoparticles
Paclitaxel

ABSTRACT

β-Cyclodextrin modified chitosan–poly(acrylic acid) nanoparticles (CS–PAACD NPs) were obtained by polymerizing acrylic acid (AA) and β-cyclodextrin (β-CD) substituted acrylic acid (AACD) in chitosan (CS) solution. These CS–PAACD NPs, characterized by transmission electron microscopy (TEM), scanning electron microscopy (SEM) as well as atomic force microscopy (AFM), were quite small in size about 40–50 nm. The size and the microstructure of these CS–PAACD NPs could be accurately controlled by changing the ration of AACD to AA. As the ratio of AACD to AA increased, the size of these NPs decreased. These as-prepared CS–PAACD NPs showed enhanced solubility for paclitaxel (PTX) in aqueous solution and exhibited a typical pH-sensitive release property for the encapsulated drug in vitro. The presence of the β-cyclodextrin inside the CS–PACD NPs greatly enhanced the ability to load hydrophobic drugs, which significantly broadened the application of CS–PAACD NPs in biomedical fields.

1. Introduction

There has been widespread interest in the study of polyelectrolyte (PEs) nanoparticles, because they are widely used in applications ranging from micro-reactors to drug and gene carriers (Hu et al., 2007; Kakizawa & Kataoka, 2002; Shchukin & Sukhorukov, 2004). Much work has been concerned with the structure control of PEs nanoparticles from di-block polyelectrolyte of polystyrene–poly(acrylic acid) (PSt–PAA), by varying factors such as block length, temperature, concentration and solvent (Zhang, Barlow, & Eisenberg, 1995; Zhang & Eisenberg, 1995, 1996a, 1996b).

However, there have been few studies focusing on controlling the micro-structure of the PEs nanoparticles using two PEs of opposite charges. Generally, when two kinds of PEs, with opposite charges, are mixed, inter-polyelectrolyte complexes (IPCs) will be formed through electrostatic interactions, perhaps strengthened by hydrophobic interactions or hydrogen bonds. The complex structure of these PEs nanoparticles depends strongly on the intrinsic stiffness and charge density of the PEs. For flexible chains with higher charge density, the PEs are close to each other and firmly complexed to form a condensed structure. On the other hand, as the chain flexibility decreases, the macroions become more linearly arranged and more separated from each other to form a loose structure (Jonssona & Linse, 2001).

In our previous work, hollow chitosan–poly(acrylic acid) (CS–PAA) PEs nanoparticles were prepared through electrostatic interactions between positively charged CS and negatively charged PAA molecules. The size and structure of these nanoparticles could be tuned by the pH value and preparation methods (Chen, Hu, Chen, Jiang, & Yang, 2005; Hu et al., 2002; Hu, Jiang, Ding, Chen, & Yang, 2004). In this work, the charge density and the chain flexibility of PAA chains was varied by substituting the neutral group of β-cyclodextrin (β-CD) with carboxyl acid through an ester bond. β-Cyclodextrin is a cyclic oligosaccharide, which consists of 7 covalently linked glucopyranose units. It has a cone-like structure, combining a hydrophilic exterior with a hydrophobic interior which can encapsulate small hydrophobic molecules or polymers to form complexes through host-guest interactions (Dong et al., 2008; Kawaguchi, Nishiyama, Okada, Kamachi, & Harada, 2000; Wang & Jiang, 2006). We find that the design of chain architecture can result in a decrease in charge density in the PAA chains, weakening the electrostatic interactions, and consequently allowing a precise control of the micro-structure of obtained PEs nanoparticles, similar to the microstructure of amphiphilic block copolymers nanoparticles prepared in aqueous solution (Chelushkin et al., 2008; Prochazka, Martin, Munk, & Webber, 1996).

These CS–PAACD NPs showed significant ability to encapsulate hydrophobic drug: paclitaxel, and pH-sensitive drug release properties in different medium. Thus pH-response drug delivery

* Corresponding authors. Fax: +86 25 83594668.
E-mail addresses: hvyong@nju.edu.cn (Y. Hu), jiangx@nju.edu.cn (X. Jiang).

0144-8617/$ – see front matter © 2012 Elsevier Ltd. All rights reserved.
http://dx.doi.org/10.1016/j.carbpol.2012.05.052

and release at tumor sites might be achieved in this system. With positive surface charges, these nanoparticles can be used as co-delivery system for anticancer drugs and plasmid, which will greatly enhance their application in biomedical fields.

2. Materials and methods

2.1. Materials

Chitosan (CS) (Nantong Shuanglin Biological Product Inc.) was refined twice as following procedure. Firstly, chitosan was dissolved in dilute acetic acid solution (1%, wt/v) and the solution was filtered with paper filter (5 μm). Then, the filtered liquor was poured into excess aqueous NaOH solution to precipitate CS. The obtained precipitation was washed with distilled water three times. Finally, the CS was dried in vacuum at room temperature for use. The deacetylation degree of CS was 88% determined by acid–base titration method (Pourjavadi, Mahdavinia, Zohuriaan-Mehr, & Omidian, 2003), and the average molecular weight of chitosan was 80 kDa determined by the viscometric method (Qurashi, Blair, & Allen, 1992). β-CD (Sinopharm Chemical Reagent Co. Ltd.) was re-crystallized from distilled water. Acryloyl chloride was from Shanghai Shunqiang Chemical Reagent Co. Ltd. and used without further purification. Acrylic acid (AA) (Shanghai Guanghua Chemical Company) was distilled under reduced pressure in nitrogen atmosphere. Potassium persulfate ($K_2S_2O_8$) was re-crystallized from distilled water. Glutaraldehyde (GA, 25%), from Sigma Chemical Company (St. Louis, MO) was used without further purification. All other reagents are of analytic grade.

2.2. Synthesis of β-CD modified chitosan–poly(acrylic acid) (CS–PAACD) nanoparticles (NPs)

Firstly, propenyl esterified β-cyclodextrin was formed directly in aqueous solution according to the literature (Harada, Furue, & Nozakura, 1976). Then, β-CD modified poly(acrylic acid)–chitosan nanoparticles (CS–PAACD NPs) were synthesized by the radical polymerization of acrylic acid (AA) and propenyl esterified β-cyclodextrin (AACD) directly in CS solution with different ratio of amino group to carboxyl group. Briefly, 0.2 g of AACD was dissolved in 50 mL H_2O, and different amounts of AA were added to it to get a series of solutions with AA:AACD (molar ratio) = 9:1, 8:1, 7:1, 6:1, 5:1, 4:1. A determined amount of CS was added to keep the molar ratio of CS vs AA (amino group vs carboxyl group) at 1.1:1. Then, this solution was heated to 70 °C till a clear solution was obtained. After that, 1.0 mg $K_2S_2O_8$ was added to the solution to initiate the polymerization under a nitrogen steam and magnetic stirring. After 1.5 h, the solution became opalescent, indicating that the polymerization was complete. The solution was then cooled to 35 °C and a known amount of GA was added to partially cross-link the amino groups of the CS with continued magnetic stirring. After 24 h with continued magnetic stirring, a light-yellow suspension was obtained. This suspension was then filtered through a cellulose acetate filter membrane (450 nm) to remove the aggregates. The residual monomers and GA were removed by dialysis against buffers (pH 4.5) using a dialysis bag (12 kDa cut off).

2.3. pH-response

The as-prepared NPs were firstly diluted by 10 times distilled water. 0.1 mL 0.6 mol/L ammonia was added to it to obtain a solution with pH around 9.5. This alkaline solution was then adjusted to various pH by adding a serial amounts of 0.2% (wt%) acetic acid solution. These suspensions were kept in vials for at least 1 h to achieve an equilibrium. The suspensions were then filtered and the stock solutions were collected for dynamic light scattering (DLS) measurements.

2.4. Preparation of PTX loaded CS–PAACD NPs

The PTX-loaded CS–PAACD NPs were prepared by a common solvent method. Briefly, 20 mg of PTX was dissolved in 2 mL ethanol to get a 10 mg/mL PTX solution. Predetermined amount of PTX–ethanol solution was dropped into 2 mL as-prepared CS–PAACD NPs suspension with different CD:PTX molar ratio under magnetic stirring and incubated for 3 days. Then, the trace ethanol was eliminated under reduced pressure and the suspension was filtered to remove non-incorporated drug crystals. The PTX-loaded nanoparticles were separated from the aqueous phase by centrifugation (TG16-W) with 12,000 rpm for 20 min. After that, these nanoparticles were lyophilized. For drug loading efficacy measurement, 1.0 mL methanol was added to 1.0 mg dried PTX-loaded particles to dissolve PTX and the concentration of PTX in the methanol was directly determined by high performance liquid chromatographic (HPLC) analysis, which was regarded as the amount that was incorporated into the CS–PAACD NPs according to the literature (Seow, Xue, & Yang, 2007). Encapsulation efficiency (EE) is defined as following:

$$\text{EE}\ \ (\%) = \frac{\text{Wieght of the drug in NPs}}{\text{Wieght of the feeding drug}} \times 100$$

The FITC (Fluorescein isothiocyanate)-labeled nanoparticles were synthesized as following. 5 mg of as prepared CS–PAACD NPs were dispersed in 1 mL sodium carbonate buffer (pH = 9.35), and 5 mg of Fluorescein isothiocyanate (FITC) was dissolved in 1 mL DMSO. Then 50 μL of this FITC solution was added to the nanoparticle suspension. The mixture was stirred for another 12 h in dark. Then, the solution was dialyzed against deionized water for three days to remove the free FITC molecules.

2.5. In vitro drug release experiment

2.0 mg of PTX loaded CS–PAACD nanoparticles was dispersed in 2.0 mL phosphate-buffered saline (PBS pH 7.4) in a dialysis bag with 12 kD molecular weight cut-off. This bag was immersed in 5 mL PBS, pH 7.4, at 37 °C with gentle agitation in an air bath incubator. Periodically, 5.0 mL release medium was collected and 5.0 mL fresh PBS was added to the system. 1.0 mL methylene dichloride (MDC) was introduced to the release medium to extract PTX. The PTX–MDC solution was separated from the water and kept in a 5.0 mL flask until MDC volatilizing out. Finally, 1.0 mL methanol was added to the flask to dissolve PTX. The concentration of PTX in methanol solution was recorded by a LC-320120AD (Shimadzu) HPLC system equipped with a Lichrospher 321C-18, 5 μm, 200 mm × 4.6 mm RP-HPLC analytical column. The mobile phase was a mixture of acetonitrile and ultra pure water (58/42, volume), and the wavelength of the ultraviolet detector was set at 227 nm. The column was eluted at a flow rate of 1.0 mL/min at 35 °C. The concentration of PTX in all samples was determined according to the peak area at retention time of 5.1 min by reference to a calibration curve.

2.6. Cell culture and in vitro cytotoxicity experiments

C6 glioma cells, from Shanghai Institute of Cell Biology were cultured in Dulbecco's Modified Eagle Media (DMEM) solution containing 10% Fetal Bovine Serum (FBS) and antibiotics (50 units/mL penicillin and 50 units/mL streptomycin) at 37 °C in 5% CO_2 environment. C6 glioma cells were seeded in 96-well plate (5×10^3 cells/well) with 200 μL DMEM medium. The medium

was changed every other day until 80% areas was covered with cells. Then 200 μL medium with PTX, blank nanoparticles, and PTX-loaded nanoparticles at different concentrations were added into these cells. PTX was dissolved in the mixture of water and DMSO (10:1, v:v) with concentration ranging from 6.25, 12.5, 25 to 50 μg/mL. Since the drug-loading content is 24.2 μg/mg, the concentrations of drug-loaded nanoparticles and blank nanoparticles were 258, 516, 1033 and 2066 μg/mL respectively. One row was used as control without addition of nanoparticles or PTX and another row was used as background without adding of cells. At different intervals, the suspension was removed and the wells were washed three times using PBS. After that, 20 μL of 3-(4,5-dimethylthiazol-2-yl)-2,5-diphenyltetrazolium bromide (MTT) assay and 180 μL of DMEM medium were added to the wells. After incubation for another 4 h, the solution was removed, leaving a precipitate. 150 μL of DMSO was added to each well before the plate was measured by a microplate reader. Cell viability was determined by the following equation:

$$\text{Cell viability}\ (\%) = \frac{I_{\text{sample}}}{I_{\text{control}}} \times 100$$

where I_{sample} and I_{control} represent the fluorescence intensity determined for cells treated with different nanoparticles and for control cells, respectively.

2.7. Cellular uptake experiments

The cellular uptake of nanoparticles was performed on both flow cytometry and laser confocal fluorescence microscopy. C6 glioma cells were seeded in a 6-well plate at a concentration of 1×10^5 cells/well. FITC-labeled CS–PAACD NPs at a concentration of 5 mg/mL were incubated with cells for 2, 4 and 12 h respectively. One well was used as control without adding of nanoparticles. For flow cytometry experiment, at determined time, the culture medium was aspirated and the cells were treated with trypsin–EDTA. Afterwards, 2 mL of PBS was added to the well, and the suspensions were then transferred to tubes and centrifuged for 5 min (1000 rpm). After aspirating the supernatant, 0.5 mL PBS was added in the tubes to suspend the cells. The fluorescence intensity of the cells was detected by a flow cytometer (BD FACS Calibur). For laser confocal fluorescence microscopy, at predetermined time intervals, the cells, co-incubated with FITC-labeled CS–PAACD, were washed by PBS (4 °C and 37 °C) for three times respectively. After that, the cells were stained with 2-(4-amidinophenyl)-6-indolecarbamidine dihydrochloride (DAPI) for 15 min, washed again with PBS for another three times, and photographed by ZEISS LSM710 laser confocal fluorescence microscopy.

2.8. Characterization

The mean diameter and size distribution of CS–PAACD NPs were determined by DLS using a Brookhaven BI9000AT system (Brookhaven Instruments Corporation, USA). The measurements were done with a wavelength of 633.0 nm at 25 °C with a detection angle of 90°. All measurements were repeated three times.

The morphology of CS–PAACD NPs was observed by transmission electron microscopy (TEM) (JEOL, TEM-100, Japan), scanning electron microscopy (SEM) (LEO 1530 VP field emission, Japan) and atomic force microscopy (AFM) (SPI3800, Seiko Instruments Inc., Japan) with tapping mode. For TEM observation, appropriately diluted samples were dripped onto a nitrocellulose covered copper grid at room temperature without staining. For SEM measurement, drops of the suspension were placed on a silicon wafer and dried in air and sputter-coated with gold before measurement. One drop of the diluted NP suspension was placed on the surface of a clean silicon wafer and dried under nitrogen flow at room temperature and observed with AFM.

FT-IR was performed through mixing lyophilized dry powder of CS–PAACD NPs with KBr and pressed it to a plate on a Bruker IFS 66 V vacuum-type spectrometer. Fluorescence measurements were performed using pyrene as fluorescent probe on Perkin Elmer (USA) LS50B fluorescence spectrometer. The concentration of NPs with different AACD:AA ratio was 1 mg/mL and pyrene retained at 6.0×10^{-7} mol/L.

3. Results and discussion

3.1. Size and morphology of CS–PAACD NPs

It was reported that the shape of PEs NPs could be tuned through monomer selection, chain architecture design, and variation of solution conditions (Kotz, Kosmella, & Beitz, 1995). Thus, in this work, we synthesized PAA chains with different chain flexibility and charge density by grafting β-CD to the PAA chain through ester bond. The mean diameter of the NPs, reflected by DLS, was changed according to the feeding molar ratio of AA:AACD. In all cases, the diameter of the NPs was less than 130 nm. When the molar ratio of AA:AACD decreased from 9:1 to 5:1, the mean diameter of these obtained CS–PAACD NPs decreased from 128 nm to 84 nm.

The morphology and microstructure of the CS–PAACD nanoparticles were measured by TEM and SEM as shown in Fig. 1a. The particle size ranges from 50 nm to 100 nm, depending on the feeding ratio of AA:AACD, which is smaller than the results observed by DLS due to the dry state in TEM observation. The size of the CS–PAACD NPs became smaller and their size distribution became more uniform when the AACD content gradually increased, indicating that the morphology of the particles was markedly dependent on the amount of β-CD grafted into the CS–PAACD NPs. When the feeding ratio of AACD:AA was about 1:9, spherical CS–PAACD NPs with dense structure (Fig. 1a) were observed. When the ratio of AACD:AA increased to 1:7, smaller nanoparticles were shown in Fig. 1b. Compared with Fig. 1a, these nanoparticles had a gray color, indicating a looser structure, because more electron beams could penetrate these nanoparticles in the TEM experiments. Further increasing the AACD content in the CS–PAACD nanoparticles, the structure of the particles transformed from a dense structure to a core-shell structure, as shown in Fig. 1c, where the particles had a quite thin shell and hollow structure in the interior. SEM image (Fig. 1d) of the hollow nanospheres also had coincident size and spherical morphology similar to the TEM observation. These results are reasonable in that the main driving forces to form CS–PAACD NPs are the electrostatic interactions between CS and PAACD. The introduction of AACD into PAA chains greatly reduced the charge density in the PAA chains, resulting in a weakness of the interactions between CS and PAACD, which affected the particle size and morphology.

Atomic force microscopy image (Fig. 2) provided further structural information of these as-prepared CS–PAACD NPs with the feeding ratio of AA:AACD at 5:1. These nanoparticles showed a spherical morphology in the height image with a size ranging from 80 to 150 nm, slightly bigger than that in the TEM results. This might be attributed to the fact that AFM measurements are based on the atomic force between the probe and the particles, and a certain space existed between them, which generated the difference of the particle size compared to TEM images. Core–shell structures were distinctly observed in the phase image (Fig. 2b). The bright shell in phase image corresponded to hard part and the dark core was attributed to soft part. Apparently, the center of nanospheres was very soft, which corresponded to the hollow structure of nanospheres as shown in the TEM images.

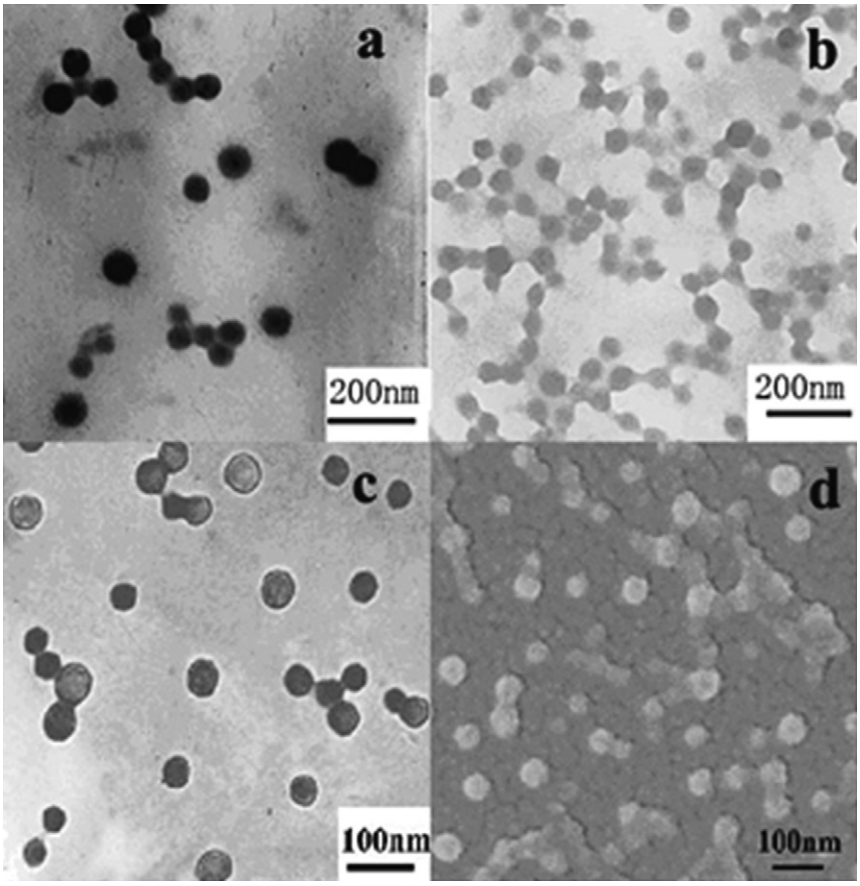

Fig. 1. TEM image of the CS–PAACD NPs with different feeding ratio of AACD:AA: (a) 1:9; (b) 1:7; (c) 1:5, and SEM image (d) of the hollow spheres in image (c).

3.2. FT-IR spectra of CS–PAACD NPs

The chemical composition of the nanoparticles with AA:AACD feeding ratio at 5:1 was thus investigated by FT-IR spectra. The IR spectrum of pure β-CD (Fig. 3a) shows predominant peaks at 3390 cm^{-1} for the OH groups, 1163 cm^{-1} for the stretching vibration of C—O—H and 1035 cm^{-1} for the C—O—C stretching vibration. In CS–PAA NPs (Fig. 3b), amino band I is at 1564 cm^{-1} and amino band II is at 1637 cm^{-1}, which are shifted to 1562 cm^{-1} and 1639 cm^{-1} in CS–PAACD NPs (Fig. 3c), respectively. The stretching vibration of C=O for carboxylic groups is also shifted from 1719 cm^{-1} to 1717 cm^{-1}. The O—C—O asymmetric stretching vibration of large cyclic ester in both chitosan and cyclodextrin can be observed at 1078 cm^{-1} and 1030 cm^{-1} in the CS–PAACD NPs. The existence of all these characteristic peaks indicated that cyclodextrin had been chemically grafted onto the PAA chains and formed complex nanoparticles with CS.

Based on above results from TEM, AFM and FT-IR spectra, it is reasonable to conclude that CS–PAACD NPs can be obtained by co-polymerization of AA and AACD in CS solution, and the microstructure of these CS–PAACD nanoparticles can be precisely controlled by carefully tuning the feeding ratio of AA to AACD.

3.3. Hydrophobic property of CS–PAACD NPs

Due to the hydrophobic property of the interior in β-CD, a small hydrophobic molecule: pyrene (Py) was used as a fluorescent probe to detect the hydrophobic property of obtained CS–PAACD NPs, because the condensed aromatics structure of Py is sensitive to polarity, producing a distinctive excimer fluorescence under conditions of sufficiently high concentration and mobility (Dong & Winnik, 1984; Kalyanasundaram & Thomas, 1977).

Fig. 4A shows the fluorescence spectra of the Py–CD complexes with a series of β-CD concentrations. It can be observed that the fluorescence intensity regularly increased with increasing CD concentration, indicating that more Py molecules are encapsulated in the CD cavity. Similar phenomenon was also observed in these CS–PAACD NPs as shown in Fig. 4B. The CD content in the CS–PAACD NPs varied from 5:1, 6:1, 7:1 to 9:1 (AA:AACD feeding ratio), which had a corresponding CD concentration of 0.620, 0.563, 0.527, 0.484 mg/mL, respectively. A significant enhancement of the Py fluorescence intensity was observed with increasing ratio of AACD:AA from 1:9 to 1:5, while the concentration of the CS–PAACD nanoparticles was fixed at 1.0 mg/mL. However, only a weak Py signal was observed in CS–PAA NPs under the same condition. This result confirmed that β-CD was inside these CS–PAACD NPs. From these results, it seems safe to draw a conclusion that the hydrophobic property of CS–PAACD NPs is mainly induced by the CDs, offering these CS–PAACD NPs the ability to load hydrophobic drugs.

3.4. pH responsibility of CS–PAACD NPs

CS–PAA nanoparticles were pH sensitive and they were stable in acidic or basic medium, and would aggregate in neutral solution (Hu et al., 2002). In this work, the introduction of CD markedly affected the stability of these CS–PAACD nanoparticles not only in acidic condition, but also in alkaline medium. Fig. 5a shows the relative light intensity (LI) as a function of the pH values with molar ratio of COOH:NH_2 fixed at 0.9, and the feeding ratio of AA:AACD is 5:1. When the pH was higher than 8.0, the LI of the suspension slightly increased with the decrease of pH value. In this stage,

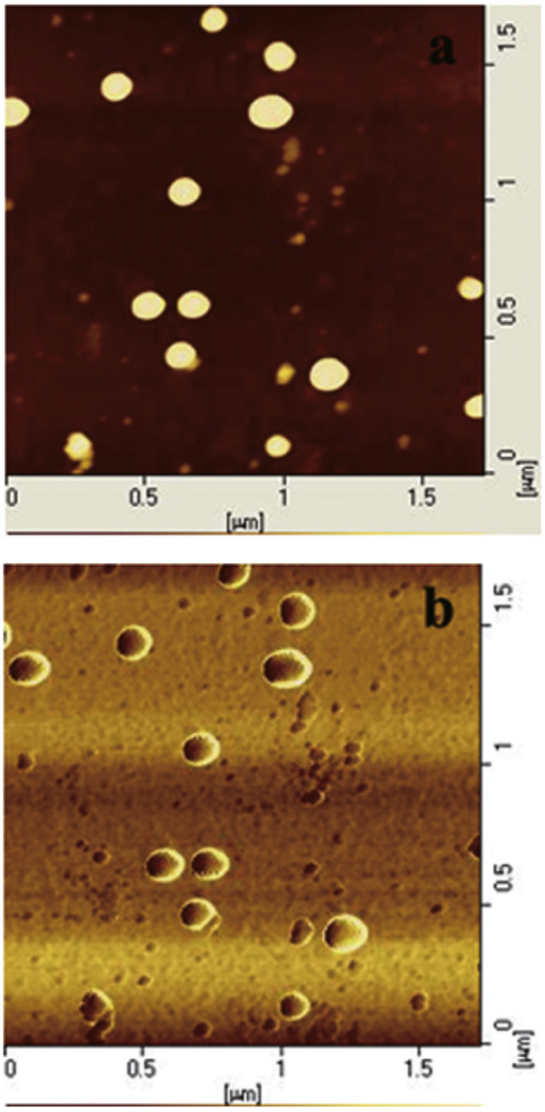

Fig. 2. AFM image of the CS–PAACD NPs. (a) Height image; (b) phase image.

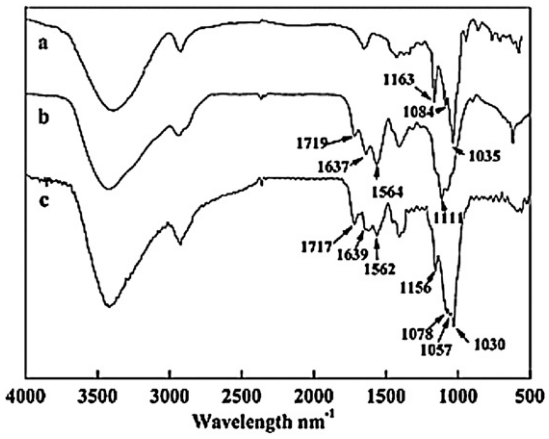

Fig. 3. FT-IR spectra of (a) cyclodextrin, (b) CS–PAA, and (c) CS–PAACD nanoparticles.

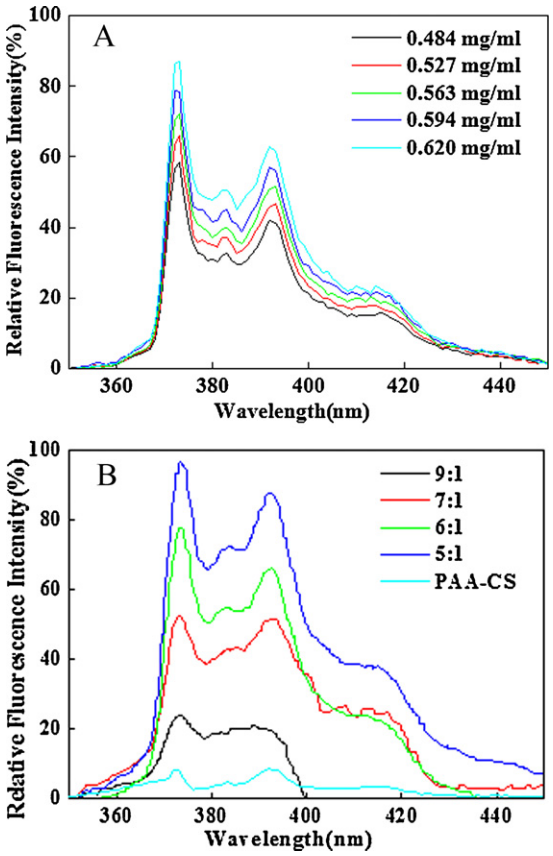

Fig. 4. Fluorescence spectra of the Py–CD complexes with different β-CD concentration (A) and Py loaded CS–PAACD NPs with different feeding molar ratio of AA vs AACD (B). The concentration of Py in each sample was fixed to be 1.0×10^{-7} mol/L and CS–PAACD NPs were fixed to be 1.0 mg/mL.

the CS–PAACD NPs separately dispersed, and the variation of pH had a small effect on the LI. When the pH value decreased from 8.0 to 7.0, LI increased rapidly at the early stage, and decreased steeply at the later stage. In this procedure, we proposed that these CS–PAACD NPs associated to form large aggregates, conferring the enhancement of the LI. After that, the size of the aggregates became bigger and bigger with further decreasing the medium pH value, consequently resulting in the sediment of the CS–PAACD NPs. During this stage, the size enlargement increased the LI, while the sediment of the CS–PAACD NPs decreased the LI. The variation of LI was attributed to the competition between these two factors. After pH < 7.0, the LI decreased sharply, and there was a sharp incline point (which was termed as flocculation point (FP)) in the LI profile around pH 6.86, indicating that all these CS–PAACD NPs deposited from the suspension at pH = 6.86. Therefore, these CS–PAACD NPs survived a suspension–congregation–flocculation variation depending on the pH.

The inset in Fig. 5a is the optical photos of the CS–PAACD NPs, which provides the macroscopic view of the congregation and flocculation procedure at different pH. Apparently, the suspension showed light-blue color under alkaline condition (pH 9.57) and the suspension became cloudy with decreased pH. When the pH was adjusted to 7.01, which was quite close to the flocculation pH (we termed flocculation pH as the isoelectric point of CS–PAACD NPs), the suspension became blue and no longer transparent as shown in the image. At the flocculation pH, deposition of the CS–PAACD NPs occurred instantly and separated from the suspension in few seconds, leaving a clear solution above the sediment. This phenomenon is quite consistent with the LI results in the DLS measurement.

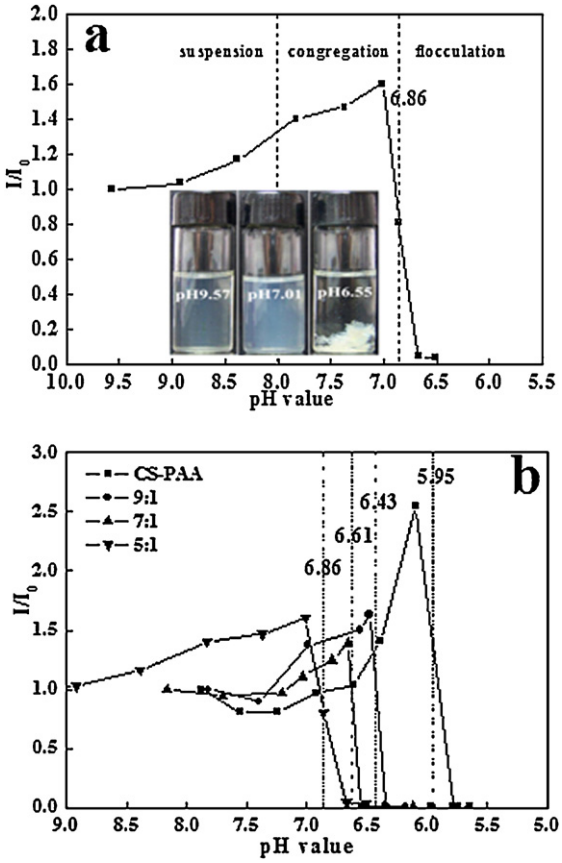

Fig. 5. Relative light intensity as a function of the pH values with different molar ratio of AA to AACD. (a) AA:AACD = 5:1 (insert is optical photos of the particles with pH = 9.57; 7.01; 6.55 respectively); (b) AA:AACD = 5:1; 7:1; 9:1 respectively. *I* and I_0 represented the light intensity at corresponding and initial pH values, respectively. The molar ratio of COOH:NH_2 was fixed to be 0.9 in each sample. (For interpretation of the references to color in the text, the reader is referred to the web version of this article.)

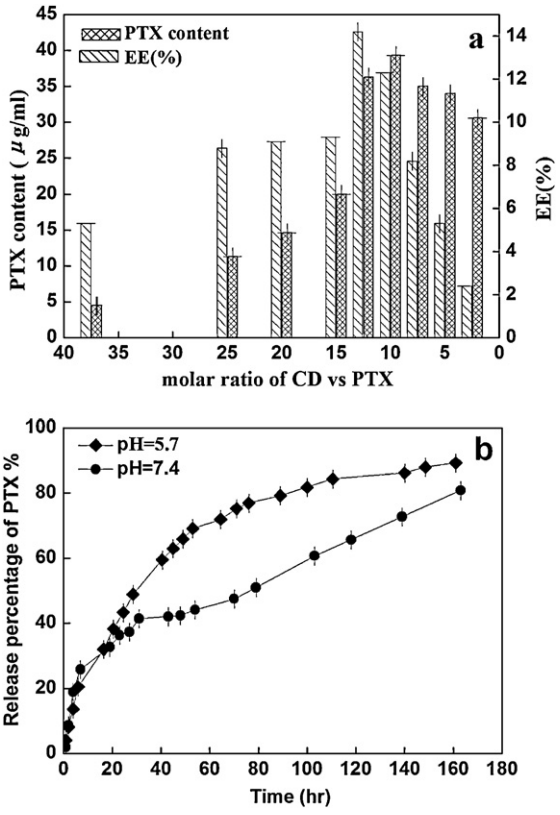

Fig. 6. Dependence of paclitaxel solubility in water and encapsulation efficiency of the CS–PAACD NPs on the molar ratio of CD:paclitaxel. Feeding ratio of AA:AACD was fixed at 5:1 in all experiments (a). The release profile of PTX from CS–PAACD NPs in the PBS with different pH value (paclitaxel concentration: 36.3 μg/mL) (b).

Fig. 5b shows that the isoelectric point of CS–PAACD NPs varied with the different amounts of introduced AACD (molar ratio of —COOH to —NH_2 is 0.9). These CS–PAACD NPs showed a positive zeta potential on the surface because of the protonation of amino groups from CS in acidic solution. The isoelectric point of CS–PAACD NPs was governed by the net charges on the surface of the CS–PAACD NPs. When more AACD was introduced into the PAA chains, the charge density of PAA chains reduced, resulting in a higher positive net charge on the surface of CS–PAACD in the medium with the same pH value. Thus more hydroxyl groups were needed to neutralize the surface charge, which shifted the isoelectric point to a higher pH value.

Malignancies show a minor decrease in extracellular pH (6.8–7.2) (Gerweck & Seetharaman, 1996). Thus, properly designed nanocarriers that are responsive to pH may be able to intelligently distinguish normal and pathological tissues, achieving better targeting efficiency and treatment efficacy. In this work, the continually tunable isoelectric point offers great opportunity to the CS–PAACD NPs when they are used as drug carriers. These NPs will be stable in plasma (pH 7.4) and deposit around the tumor site (pH 6.8–7.2), realizing the pH-induced targeted therapy stratagem.

3.5. PTX loading and release from CS–PAACD NPs

The hydrophobic interior of β-CD can encapsulate PTX molecules and significantly enhances the solubility of PTX in water through host-guest interactions and maintains its biological activity in vitro (Qurashi et al., 1992). Enhanced water solubility of PTX in aqueous solution by CS–PAACD NPs suspension was shown in Fig. 6a. The PTX content showed a parabola-like increase with the molar ratio of CD:PTX varying from 37.5:1 to 2.5:1. Introduction of β-CD into CS–PAA nanoparticles could indeed enhance the solubility of PTX and the enhancing ability depended on the ratio of β-CD to PTX. Highest concentration of PTX was achieved when the feeding ratio of β-CD:PTX was 10:1. At this point, the concentration of PTX was 39.3 μg/mL, 115-fold higher than that in pure water. The dependence of encapsulation efficiency (ee%) of PTX with the CD:PTX molar ratio was also showed in Fig. 6a. When the β-CD:PTX increased from 2.5:1 to 12.5:1, the encapsulation efficiency increased linearly. The highest encapsulation efficiency in our system reached about 14% (PTX content: 36.3 μg/mL). Then this value reduced while the CD moiety continued increasing. So the drug release measurement in vitro was performed at β-CD:PTX = 12.5:1.

The cumulative release of PTX from CS–PAACD NPs under simulated physiological condition (PBS, pH 7.4) and at pH 5.7 over a period of time was shown in Fig. 6b. The in vitro drug release profiles of PTX showed a sustained manner for more than one week for both cases. As the drug-loaded sample was immersed in phosphate buffer solution (PBS, pH 7.4) at 37 °C, after an initial burst release of PTX, these CS–PAACD NPs provided a linear releasing profile for the PTX. The release rate of PTX-loaded CS–PAACD NPs also depended on the pH value in this procedure. PTX released faster in the medium of pH 5.7 than that in pH 7.4. This property might be interesting in the therapy of tumor disease. As we know that the plasma of human is neutral (pH 7.4), while the pH near the tumor is weakly acidic, the different release behaviors under these two conditions make it

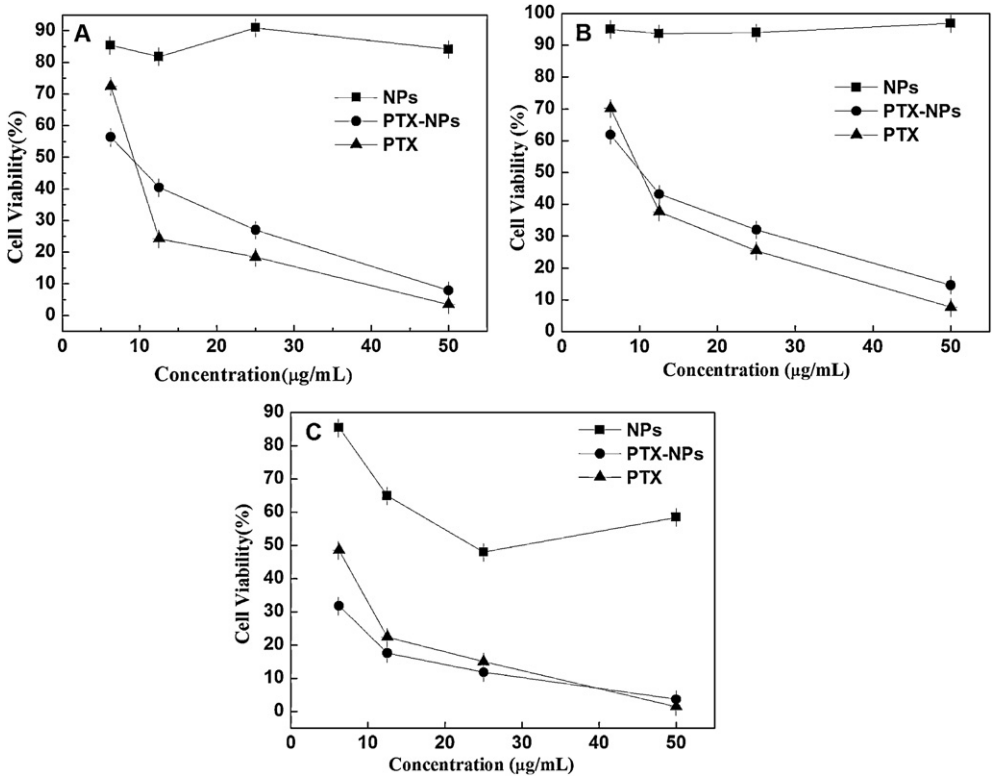

Fig. 7. Cell Viability of the C6 glioma cells incubated with free PTX, PTX-loaded CS–PAACD nanoparticles and blank CS–PAACD nanoparticles for 24 h (A), 48 h (B), and 72 h (C) by MTT assay.

possible for more drugs to be released in the tumors. In addition, these CS–PAACD NPs are pH sensitive and will subside around the tumor site. Thus these drug-loaded CS–PAACD NPs could targeted deliver anti-tumor drugs to the pathologic area and release them in situ.

3.6. Cell viability and uptaken

The cytotoxicity is an important issue for both the drug and the carrier. Although, chitosan and β-CD are reported as promising biomaterials, safely used in drug delivery system, the cytotoxicity

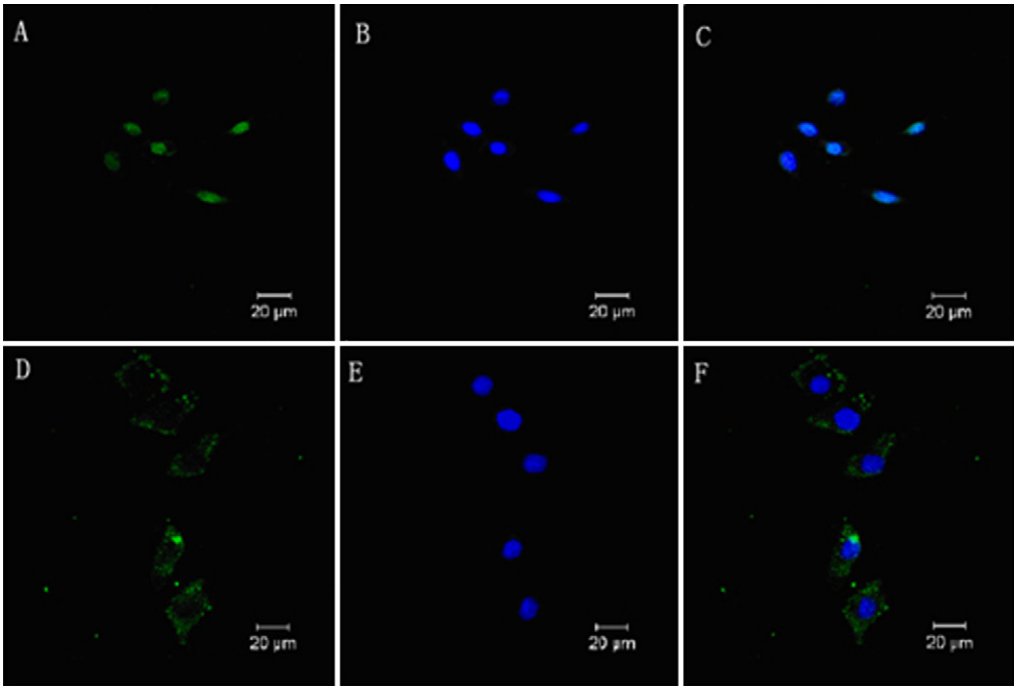

Fig. 8. Laser confocal fluorescence microscopies of C6 glioma cells incubated with FITC-labeled nanoparticles for 2 h (A–C), 4 h (D–F); cytoplasma lighten by FITC (A and D), nucleus stained by DAPI (B and E), and the merge images with the differential luminous signs (C and F). (For interpretation of the references to color in the text, the reader is referred to the web version of this article.)

against C6 glioma cells among blank CS–PAACD NPs, pure PTX and PTX-loaded CS–CDPAA NPs are re-examined. Fig. 7A shows the cytotoxicity of these three kinds of sample after incubation with C6 glioma cells for 24 h by MTT assay. It clearly showed that blank CS–PAACD nanoparticles almost had no cytotoxicity against C6 glioma cells within the measured concentrations during the incubation time. However, for the PTX and PTX loaded nanoparticles, the cell viabilities decreased rapidly with the increase of the PTX concentration. Furthermore, compared with the cytotoxicity of free PTX, PTX loaded CS–PAACD NPs showed a slightly lower cytotoxicity in most tested concentrations. This can be attributed to the sustained release property of PTX from these CS–PAACD NPs. Only part of the total encapsulated PTX released from the CS–PAACD NPs during 24 h, resulting in a reduced cytotoxicity. After incubation for 48 h, the free PTX also showed higher cytotoxicity than CS–PAACD NPs against C6 glioma cells (Fig. 7B). However, on the third day, the cell viability treated with PTX loaded CS–PAACD NPs showed a better cytotoxicity over the free DOX (Fig. 7C). At this point, the amount of the PTX released from the NPs is high enough to suppress the proliferation of the C6 glioma cells. The higher cytotoxicity from CS–PAACD NPs might be attributed to the effective cell uptake efficiency (Yan et al., 2009).

From the in vitro cytotoxicity experiment, we hypothesized that more PTX loaded CS–PAACD NPs were taken up by C6 glioma cells with extending incubation time. Therefore, the fluorescence intensity of the FITC labeled CS–PAACD NPs over 2, 4 and 12 h was investigated by flow cytometry. With 2 h incubation, the fluorescent intensity of FITC labeled CS–PAACD NPs is 134. After 4 h incubation, the fluorescent intensity reaches 246, which clearly indicates that the internalization of CS–PAACD NPs is time-dependent. However on further extending the incubation time to 12 h, the fluorescent intensity did not increase significantly, which can be attributed to the bleaching of the FITC immersed long time in the cell culture medium. The variation of fluorescent intensity inside the cells confirmed that more CS–PAACD NPs could be taken up by C6 glioma cells with extending incubation time.

The cellular uptake of CS–PAACD NPs was also examined by laser confocal fluorescence microscopy as shown in Fig. 8. The green part indicated FITC-labeled nanoparticles, and blue represented the nucleus stained with 4′,6-diamidino-2-phenylindole, 2-(4-amidinophenyl)-1H-indole-6-carboxamidine (DAPI) dye. Within the first 2 h, only a blurry green color was observed inside the cytoplasma, and nucleus showed blue color because of the staining of the DAPI. After 4 h incubation, stronger green fluorescent signal was observed in the C6 glioma cell. No green color was seen inside the nucleus, which indicated that these internalized NPs could not penetrate into the nucleus. These results also agree with the flow cytometry results which suggested that the cell uptake efficacy is time-dependent.

4. Conclusions

By moderately adjusting the feeding ratio of monomers, β-CD modified chitosan–poly(acrylic acid) NPs with different size and structure were successfully synthesized by radical polymerization in aqueous solution. With high β-CD moiety, core-shell nanoparticles with only 40–50 nm in diameter were obtained. These β-CD modified CS–PAACD NPs showed a pH dependent stability in the solution. When decreasing the pH of the suspension from alkaline to acidic condition, the nanoparticles would gradually aggregate and flocculate from the mother liquor. The flocculation pH could be controlled by adjusting the feeding ration of AA:AACD. These nanoparticles collapsed at pH = 6.8 when the molar ratio of amino groups versus carboxyl groups was 0.9, which was just the extracellular pH point of most tumors. Meanwhile, the introduction of β-CD into these nanoparticles greatly enhanced the solubility of PTX in water. These loaded PTX could be released in a controlled manner in vitro in PBS buffer with different pH values. Thus foreseeable pH-response anticancer drug delivery and accumulative drug release at tumor sites might be realized in this system. Furthermore, considering their positive surface charges, these CS–PAACD NPs will be a potential delivery platform both for anticancer drugs and genes.

Acknowledgments

This work is supported by the National Natural Science Foundation of China (Nos. 21074051, 51033002, 21105047 and 20874042), and the Provincial Natural Science Foundation of Jiangsu Province (BK2010301).

References

Chelushkin, P. S., Lysenko, E. A., Bronich, T. K., Eisenberg, A., Kabanov, V. A., & Kabanov, A. V. (2008). Polyion complex nanomaterials from block polyelectrolyte micelles and linear polyelectrolytes of opposite charge. 2. Dynamic properties. *Journal of Physical Chemistry B*, *112*, 7732–7738.

Chen, Q., Hu, Y., Chen, Y., Jiang, X. Q., & Yang, Y. H. (2005). Microstructure formation and property of chitosan–poly(acrylic acid) nanoparticles prepared bymacromolecular complex. *Macromolecular Bioscience*, *5*, 993–1000.

Dong, H. Q., Li, Y. Y., Cai, S. J., Zhuo, R. X., Zhang, X. Z., & Liu, L. J. (2008). A facile one-pot construction of supramolecular polymer micelles from β-cyclodextrin and poly(ε-caprolactone). *Angewandte Chemie International Edition*, *47*, 5573–5576.

Dong, D. C., & Winnik, M. A. (1984). The Py scale of solvent polarities. *Canadian Journal of Chemistry*, *62*, 2560–2565.

Gerweck, L. E., & Seetharaman, K. (1996). Cellular pH gradient in tumor versus normal tissue: Potential exploitation for the treatment of cancer. *Cancer Research*, *56*, 1194–1198.

Harada, A., Furue, M., & Nozakura, S. I. (1976). Macromolecules cyclodextrin-containing polymers. I. Preparation of polymers. *Macromolecules*, *9*, 701–704.

Hu, Y., Ding, Y., Ding, D., Sun, M. J., Zhang, L. Y., Jiang, X. Q., et al. (2007). Hollow chitosan/poly(acrylic acid) nanospheres as drug carriers. *Biomacromolecules*, *8*, 1069–1076.

Hu, Y., Jiang, X. Q., Ding, Y., Chen, Q., & Yang, C. Z. (2004). Core-template-free strategy for preparing hollow nanospheres. *Advanced Materials*, *16*, 933–937.

Hu, Y., Jiang, X. Q., Ding, Y., Ge, H. X., Yuan, Y. Y., & Yang, C. Z. (2002). Synthesis and characterization of chitosan–poly(acrylic acid) nanoparticles. *Biomaterials*, *23*, 3193–3201.

Jonssona, M., & Linse, P. (2001). Polyelectrolyte–macroion complexation. II. Effect of chain flexibility. *Journal of Chemical Physics*, *115*, 10975–10985.

Kakizawa, Y., & Kataoka, K. (2002). Block copolymer micelles for delivery of gene and related compounds. *Advanced Drug Delivery Reviews*, *54*, 203–222.

Kalyanasundaram, K., & Thomas, J. K. (1977). Environmental effects on vibronic band intensities in pyrene monomer fluorescence and their application in studies of micellar systems. *Journal of the American Chemical Society*, *99*, 2039–2044.

Kawaguchi, Y., Nishiyama, T., Okada, M., Kamachi, M., & Harada, A. (2000). Complex formation of poly(ε-caprolactone) with cyclodextrins. *Macromolecules*, *33*, 4472–4477.

Kotz, J., Kosmella, S., & Beitz, T. (1995). Self-assembled polyelectrolyte systems. *Progress in Polymer Science*, *26*, 1199–1232.

Pourjavadi, A., Mahdavinia, G. R., Zohuriaan-Mehr, M. J., & Omidian, H. J. (2003). Modified chitosan. I. Optimized cerium ammonium nitrate-induced synthesis of chitosan-graft-polyacrylonitrile. *Journal of Applied Polymer Science*, *88*, 2048–2054.

Prochazka, K., Martin, T. J., Munk, P., & Webber, S. E. (1996). Polyelectrolyte poly(tert-butyl acrylate)-block-poly(2-vinylpyridine) micelles in aqueous media. *Macromolecules*, *29*, 6518–6525.

Qurashi, M. T., Blair, H. S., & Allen, S. J. (1992). Studies on modified chitosan membranes. I. Preparation and characterization. *Journal of Applied Polymer Science*, *46*, 255–261.

Seow, W. Y., Xue, J. M., & Yang, Y. Y. (2007). Targeted and intracellular delivery of PTX using multi-functional polymeric micelles. *Biomaterials*, *28*, 1730–1740.

Shchukin, D. G., & Sukhorukov, G. B. (2004). Nanoparticle synthesis in engineered organic nanoscale reactors. *Advanced Materials*, *16*, 671–682.

Wang, J., & Jiang, M. J. (2006). Polymeric self-assembly into micelles and hollow spheres with multiscale cavities driven by inclusion complexation. *Journal of the American Chemical Society*, *128*, 3703–3708.

Yan, E. Y., Ding, Y., Chen, C. J., Li, R. T., Hu, Y., & Jiang, X. Q. (2009). Polymer/silica hybrid hollow nanospheres with pH-sensitive drug release in physiological and intracellular environments. *Chemical Communications*, *19*, 2718–2720.

Zhang, L. F., Barlow, R. J., & Eisenberg, A. (1995). Scaling Relations and Coronal Dimensions in Aqueous Block Polyelectrolyte Micelles. *Macromolecules*, *28*, 6055–6066.

Zhang, L. F., & Eisenberg, A. (1995). Multiple morphologies of crew-cut aggregates of polystyrene-b-poly(acrylic acid) block copolymers. *Science*, *268*, 1728–1731.
Zhang, L. F., & Eisenberg, A. (1996a). Morphogenic effect of added ions on crew-cut aggregates of polystyrene-b-poly(acrylic acid) block copolymers in solutions. *Macromolecules*, *29*, 8805–8815.
Zhang, L. F., & Eisenberg, A. (1996b). Multiple morphologies and characteristics of crew-cut micelle-like aggregates of polystyrene-b-poly(acrylic acid) diblock copolymers in aqueous solutions. *Journal of the American Chemical Society*, *118*, 3168–3181.